Fivefold confinement time increase in the Madison Symmetric Torus using inductive poloidal current drive[*]

M. R. Stoneking,[†,a)] N. E. Lanier, S. C. Prager, J. S. Sarff, and D. Sinitsyn
Department of Physics, University of Wisconsin—Madison, Madison, Wisconsin 53706

Current profile control is employed in the Madison Symmetric Torus [R. N. Dexter *et al.*, Fusion Technol. **19**, 131 (1991)] reversed field pinch to reduce the magnetic fluctuations responsible for anomalous transport. An inductive poloidal electric-field pulse is applied in the sense to flatten the parallel current profile, reducing the dynamo fluctuation amplitude required to sustain the equilibrium. This technique demonstrates a substantial reduction in fluctuation amplitude (as much as 50%), and improvement in energy confinement (from 1 to 5 ms); a record low fluctuation (0.8%) and record high temperature (615 eV) for this device were observed simultaneously during current drive experiments. Plasma beta increases by 50% and the Ohmic input power is three times lower. Particle confinement improves and plasma impurity contamination is reduced. The results of the transient current drive experiments provide motivation for continuing development of steady-state current profile control strategies for the reversed field pinch. © *1997 American Institute of Physics.* [S1070-664X(97)91905-4]

I. INTRODUCTION AND MOTIVATION

Local measurements of fluctuation induced transport across the confining field of the reversed field pinch (RFP) have identified magnetic turbulence as the principal cause of anomalous particle[1] and energy[2] loss (inside $r/a = 0.85$). The dominant fluctuations are understood to result from internally resonant resistive tearing instabilities,[3,4] the drive for which is the gradient in the current density.[5–7]

The experiments reported in this article were designed as a test of the effects of current profile modification in the RFP. Current profile control has been proposed to reduce the magnetic turbulence that drives transport. The proposals employ auxiliary electrostatic,[8] rf,[9,10] or neutral beam[11] current drive to flatten the current profile and reduce the free energy for the tearing instability. The current profile control tests in the Madison Symmetric Torus (MST) make use of an inductive electric-field pulse to transiently drive poloidal current. During the applied pulse, we observe a robust reduction of the magnetic fluctuations and a coincident improvement in particle and energy confinement. The results provide confirming evidence that RFP transport is governed by magnetic turbulence and encourage pursuit of noninductive current profile control strategies for improving the RFP concept.

The RFP configuration is maintained by application of a toroidal electric field that tends to peak the current profile due to the shear in the magnetic field. At the $q = 0$ surface, for example, the applied electric field is perpendicular to the local magnetic field. The peaked current profile drives resistive tearing instabilities that redistribute the input electromagnetic energy and drive poloidal (i.e., parallel) current at the edge of the plasma sustaining the equilibrium. This effect is the so-called RFP dynamo, and in the MST dynamo activity is observed in both a continuous background form and in

periodic, discrete bursts or ''sawteeth.''[12] The fluctuations responsible for the dynamo (internally resonant, poloidal mode number $m = 1$ tearing modes) are also responsible for the observed anomalous transport.[1,2] The goal of auxiliary current drive for confinement improvement is to tailor the externally applied parallel electric field to match $\eta J_\parallel$, obviating the need for the dynamo fluctuations. The experiments reported here represent the first step in this program.

In Sec. II, we describe the experimental technique. The observation of fluctuation reduction and confinement improvement are presented in Sec. III, with a description of the model used to determine the time-dependent Ohmic heating power. The same model provides information on the modification to the current profile that occurs with the auxiliary drive (Sec. IV). A summary of the main results are given in Sec. V.

II. EXPERIMENTAL TECHNIQUE

The Madison Symmetric Torus ($R = 1.5$ m, $a = 0.52$ m) is operated as a reversed field pinch. Previous papers describe the device,[13] the global confinement properties of MST discharges,[14] and the scaling of confinement with control parameters.[15] Except where noted, the results reported here were obtained at toroidal plasma current, $I_\phi \approx 340$ kA, and the central line averaged density, $n_e \approx 1.0 \times 10^{19}$ m^{-3}.

To drive poloidal current, a series of four poloidal electric-field pulses are generated during the current flattop by application of voltage (V_θ) pulses to the toroidal field coil from four capacitor banks triggered independently (Fig. 1). We refer to this technique as pulsed poloidal current drive (PPCD). In previously reported PPCD experiments,[16] a single large pulse was used. With the upgraded four-pulse circuit, the transition to the current drive phase is more gradual, reducing impurity influx due to enhanced wall interaction, and the current drive period is extended up to ~10 ms, of order or longer than the transport time scale. In addition, a new extremely low amplitude fluctuation period phe-
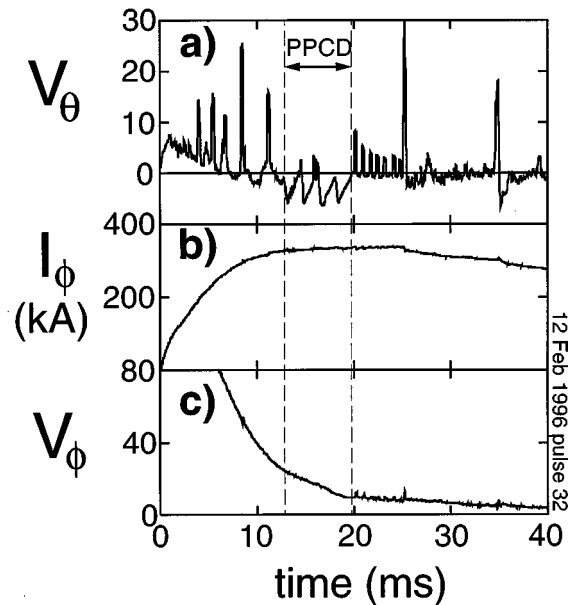

FIG. 1. (a) Poloidal loop voltage for a discharge with current profile control applied at 13 ms, along with (b) toroidal plasma, and (c) toroidal loop voltage.

nomenon has been observed with the upgraded circuit. The transition to this low fluctuation period is not precisely understood, but the energy confinement is highest when the fluctuations are minimum. The sharp positive spikes seen in Fig. 1 prior to and following application of PPCD result from discrete dynamo (flux generation) events, hereafter referred to as ''sawteeth.'' The V_θ spikes represent the toroidal field circuit's inductive back reaction to internally generated flux, and they oppose the natural current profile flattening associated with sawteeth.[17] In contrast, PPCD is an externally applied poloidal electric field with the sense required to flatten the parallel current density profile.

III. FLUCTUATION REDUCTION AND CONFINEMENT IMPROVEMENT

A. Magnetic fluctuations

The dominant fluctuations in the RFP are saturated, internally resonant resistive tearing modes. In MST, the tearing modes propagate presumably due to $\mathbf{E} \times \mathbf{B}$ and diamagnetic drifts giving them Doppler shifted frequencies in the range 10–20 kHz. Fluctuation measurements are made with an array of 32 toroidally separated poloidal field pickup coils attached to the vacuum vessel wall and spanning the entire toroidal circumference. Toroidal mode numbers $n \leqslant 15$ are resolved. The total rms fluctuation amplitude $\widetilde{b}_{rms} = \sqrt{\widetilde{b}_\theta^2 + \widetilde{b}_\phi^2}$ at the plasma surface is obtained using the curl-free condition, $\mathbf{k} \times \widetilde{\mathbf{b}} = 0$ and the fact that the dominant modes are $m = 1$, to relate the toroidal field amplitude to the measured poloidal field amplitude of each mode. Past measurements have confirmed the $m = 1$ polarization of the dominant fluctuations and the radial component is negligible, since the plasma is bounded by a close-fitting conducting shell.
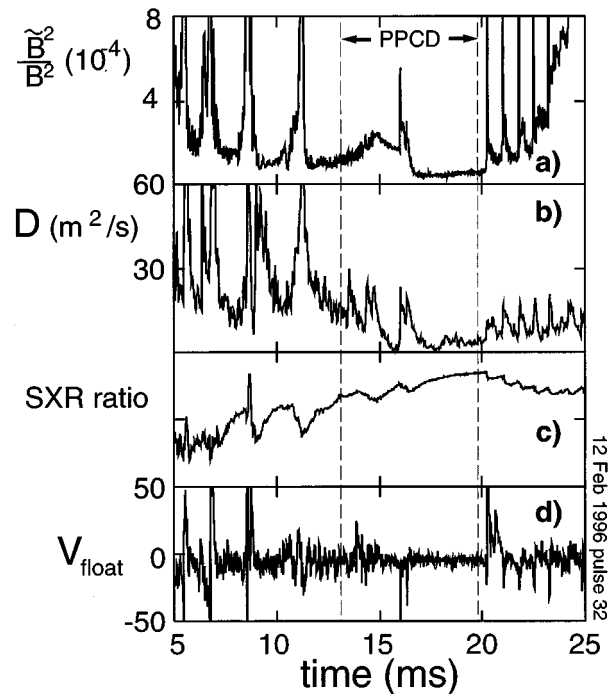

FIG. 2. (a) Mean-squared magnetic fluctuations at the plasma surface, (b) estimated global particle diffusion coefficient, (c) ratio of beryllium filtered surface barrier diode signals indicating central electron temperature, and (d) the raw floating potential signal from a Langmuir probe during a discharge with PPCD applied at 13 ms.

Figure 2 shows the mean-squared fluctuation level at the plasma surface during the same discharge as shown in Fig. 1. Prior to application of PPCD, the fluctuation bursts associated with sawteeth are observed. In general, during the PPCD phase, the fluctuation amplitude is maintained at the low level realized between sawteeth. However, in the discharge shown, there is a spontaneous transition to an extremely low fluctuation level. Such transitions occur in a subset of PPCD discharges. Following the current drive phase, there are a sequence of small amplitude sawteeth prior to a very large sawtooth crash. The small amplitude sawteeth are frequently observed during the PPCD phase as well as immediately following it. They have a different spectral content than ordinary sawteeth (with $m = 1$ precursors), are not as detrimental to confinement, and may act as the trigger event for the transition to the low fluctuation period by locally modifying the current profile. Also shown is an estimate of the global particle diffusion coefficient (discussed below), the ratio of two soft x-ray detector signals with different filter thicknesses (Be 0.3 and 0.6 μm), and the floating potential signal from a Langmuir probe at the edge of the plasma. These signals are shown to indicate the remarkable correlation between magnetic fluctuations and all other indicators of turbulence and confinement. The source of the soft x-ray emission is bremsstrahlung radiation as well as high charge state impurity lines (e.g., OVIII) that are only excited at high temperatures. The ratio of the signal with two different filters is an indicator of electron temperature. Coincident with the decrease in the magnetic fluctuation level, the three entirely independent measurements show reduced edge tur-
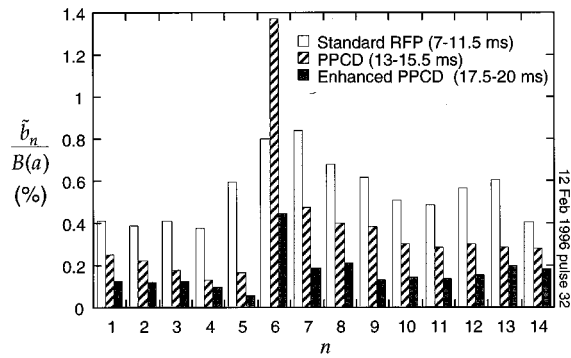
FIG. 3. Toroidal mode number spectra averaged over three time periods to indicate changes in the fluctuation spectrum during PPCD and PPCD with extremely low fluctuations.
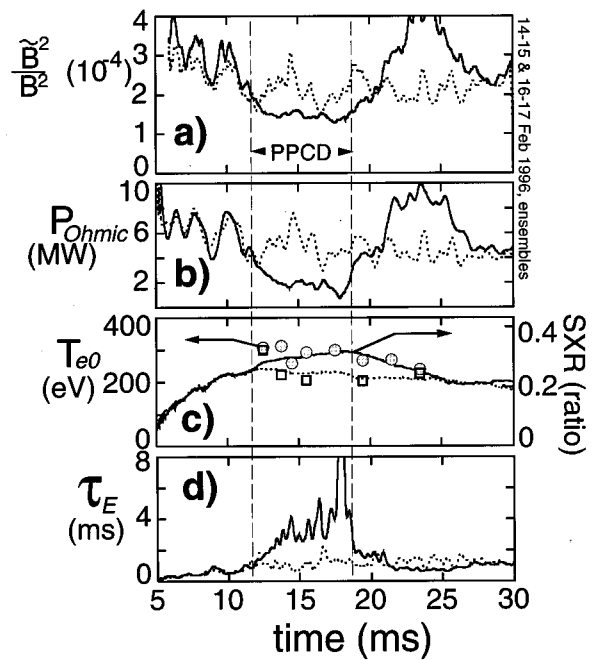

FIG. 4. Signals averaged over ensembles of standard RFP discharges (dashed) and discharges with PPCD applied (solid): (a) mean-squared magnetic fluctuation, (b) Ohmic heating power, (c) central electron temperature measured with Thomson scattering (filled circles are with PPCD, open squares without PPCD) and the ratio of two filtered soft x-ray detector signals, (d) energy confinement time calculated using the scaled ratio of soft x-ray signals to get a time-resolved electron temperature.

bulence ($\widetilde{V}_{\text{float}}$), increased central electron temperature (SXR), and improved global particle confinement (D).

The dominant toroidal mode number fluctuations in MST are $n=6$, 7, and 8. The $n=5$ mode is frequently present with an ''inverse sawtooth'' variation, suggesting it passes into and out of resonance, and therefore, that the on-axis value for the safety factor, $q=rB_\phi/RB_\theta$, hovers around 0.2. In Fig. 3, toroidal mode number spectra averaged over three time intervals are compared. The spectrum averaged from 7.0 to 11.5 ms is typical of the spectrum averaged over the sawtooth cycle and illustrates the contribution of many modes to the total fluctuation. After PPCD is applied at $\sim$12 ms, all mode amplitudes are significantly reduced, except for the $n=6$, which is somewhat larger. The spectrum is dominated by the $n=6$ single helicity during this phase. During the extremely low fluctuation period (17.5–20.0 ms), all the dominant mode amplitudes are reduced, including the $n = 6$. The dominance of the single mode in the standard PPCD spectrum is not understood, but likely depends on details of the current profile that are not experimentally accessible with the present diagnostic set.

B. Plasma beta and energy confinement

Fluctuation reduction and confinement improvement are robust features of discharges with inductive poloidal current drive. Figure 4 shows the results of averaging 100 discharges (solid curves). The only shot selection for the average was done to assure relatively uniform plasma current and density in the shot set. The dashed curves are averages over $\sim$60 standard RFP discharges with comparable toroidal plasma current and density. Panel (a) shows the robust suppression of magnetic fluctuations with the auxiliary current profile control, at the level generally observed between sawteeth. The Ohmic heating power is reduced by a factor of $\sim$3 [panel (b)] and represents the largest contribution to the improved confinement time measurement. Calculation of the time-dependent heating power is discussed below.

The stored thermal energy in the plasma is measured with a single point, single pulse Thomson scattering diagnostic (T_{e0}), a neutral (charge exchange) energy analyzer (T_i), and an 11 chord far-infrared (FIR) interferometer [$n_e(r)$]. Temporal information on the electron temperature

is acquired by varying the trigger time for the Thomson scattering laser on a shot by shot basis. The results of these measurements show that electron temperature is increased by 50% when PPCD is applied. For each point in panel (c), Thomson scattered spectra from $\sim$12 discharges were accumulated to improve the fitting uncertainty. Uncertainties are comparable to the symbol size. Overlaid with the electron temperature is the filtered soft x-ray signal ratio, providing an indication of electron temperature with good time resolution. The ratio shows a similar increase to the Thomson scattering measured T_e. Neither the majority proton temperature (charge exchange energy analyzer) nor the core impurity ion species temperature (Doppler spectroscopy of carbon V) show significant change with application of PPCD. For these discharge conditions, $T_i \approx 115$ eV. The standard RFP control set discharges were chosen to have comparable density to those with PPCD (see Fig. 7 for shot averaged density traces). The last panel in Fig. 4 gives an indication of the temporal behavior of the energy confinement time. Since the temporal resolution on the electron temperature measurement is coarse, the confinement time in Fig. 4(d) was calculated using the ratio of the soft x-ray signals shown in Fig. 4(c), scaled to agree with the Thomson scattering measurements. The magnitude of the oscillations in τ_E give an indication of the uncertainty ($\sim$1 ms) in the confinement numbers quoted below. Confinement degrades following the PPCD phase even relative to standard RFP discharges. This reflects the reproducible occurrence of large sawtooth events immediately following PPCD. The elevated magnetic fluctuation level seen in Fig. 4(a) (from 20 to 25 ms) due to

	Standard RFP	PPCD
Plasma current, I_ϕ	340 kA	340 kA
Density, n_e	1.0×10^{19} m^{-3}	1.0×10^{19} m^{-3}
Temperature, T_{e0}	230 eV	390 eV
Beta, β_θ	6%	9%
Heating power, P_{Ohmic}	4.4 MW	1.3 MW
Fluctuation, $\tilde{b}_{\text{rms}}/B(a)$	1.5%	0.8%
Confinement, τ_E	1 ms	5 ms

sawtooth activity results in enhanced transport (higher Ohmic input power).

For the shot ensembles shown in Fig. 4, the poloidal beta $\beta_\theta \equiv 2\mu_0\langle nk_BT\rangle/B_\theta(a)^2$ in the middle of the poloidal current drive phase (17 ms) is 8% compared to 6% without PPCD at the same time. The energy confinement time reaches ~4 ms with PPCD compared to 1 ms in standard RFP discharges. Parabolic pressure profiles were used for the beta and confinement calculations. The measured density profile from 11 chords of interferometry is generally flatter than parabolic, but no profile information is available on the temperature. When shots with extremely low fluctuation periods are ensembled (like those in Fig. 2), the poloidal beta reaches 9% and the confinement time rises to 5 ms (±1 ms), five times the confinement observed in standard RFP discharges. Table I summarizes the confinement numbers for standard discharges and the PPCD case with very low magnetic fluctuations.

Extremely low fluctuation events similar to Fig. 2 have been observed in higher plasma current (450 kA) PPCD plasmas. The highest electron temperature recorded in MST (615 eV) was observed in these discharges, and the confinement time is comparable to or higher than the 5 ms value measured at 340 kA, although the uncertainty is larger.

C. Time-dependent Ohmic input power

The experiments reported here are transient and make use of a changing toroidal flux in the plasma volume to generate a parallel electric field. To assess changes in the energy confinement time, it is necessary to carefully track changes in the stored magnetic energy to determine the time-resolved heating power or Ohmic dissipation. This calculation is especially important in light of the observation that much of the inferred confinement improvement comes from a drop in the Ohmic input power, despite a relatively constant Poynting flux into the plasma (when compared to discharges without application of PPCD).

From global power balance, the Ohmic heating power is

$$P_{\text{Ohmic}}=V_\phi I_\phi+V_\theta I_\theta-\frac{d}{dt}\left(\frac{1}{2}LI_\phi^2\right). \tag{1}$$

The first two terms on the right-hand side of Eq. (1) make up the integrated Poynting flux entering the plasma from the external circuit. The second term on the right-hand side is the changing stored magnetic energy; it is the inductive correc-
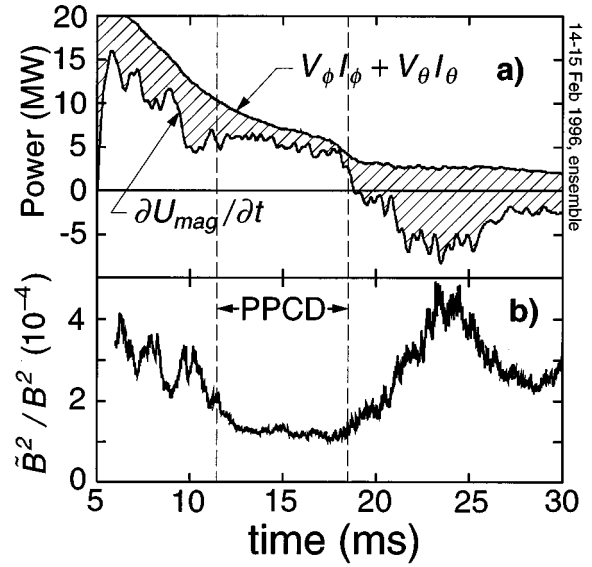

FIG. 5. (a) The integrated Poynting flux into the plasma volume (top curve) for an ensemble of discharges with PPCD and the model calculated time derivative of the stored magnetic energy. Shading indicates the time-dependent Ohmic heating power. (b) Mean-squared magnetic fluctuation shown to illustrate the correlation between low Ohmic power and low fluctuations.

tion to the heating power. The energy confinement time is calculated, taking account of changes in the thermal energy

$$\tau_E=\frac{3\int nk_BTdV/2}{P_{\text{Ohmic}}-d/dt(3\int nk_BTdV/2)}. \tag{2}$$

The top curve in Fig. 5(a) shows the integrated Poynting flux into the plasma volume (shot averaged). The time derivative of stored magnetic energy is calculated from the field model described below. The dissipated (or Ohmic heating) power, the difference between the two curves (hatched), is significantly reduced during the current drive phase. The power added to the plasma through the auxiliary current drive circuit is included in the Poynting power (through $V_\theta I_\theta$), but is a small fraction (~1 MW) of the total input power.

Since the toroidal plasma current is constant during the current drive phase (Fig. 1), the change in magnetic energy is primarily a change in inductance. The inductance change is calculated using a cylindrical, four-parameter magnetic-field model. The model is a solution of Ampère's law and equilibrium force balance with the following parametrization of the current density:

$$(\boldsymbol{\nabla}\times\mathbf{B})/\mu_0=\lambda_0(1-(r/a)^\alpha)\mathbf{B}+\mathbf{B}\times\boldsymbol{\nabla}p/B^2. \tag{3}$$

The pressure profile is assumed to be parabolic, and the peak value is adjusted to agree with the measured poloidal beta, $\beta_\theta=2\mu_0\langle p\rangle/B_{\theta a}^2$. The model is further constrained by measurements of the toroidal plasma current, the toroidal magnetic flux, and the toroidal field at the plasma surface. An independent check of the model was performed by comparing the measured poloidal asymmetry factor, Λ, with the model's prediction. Figure 6 (top curve) shows the behavior of the asymmetry factor measured with set of 16 field sens-

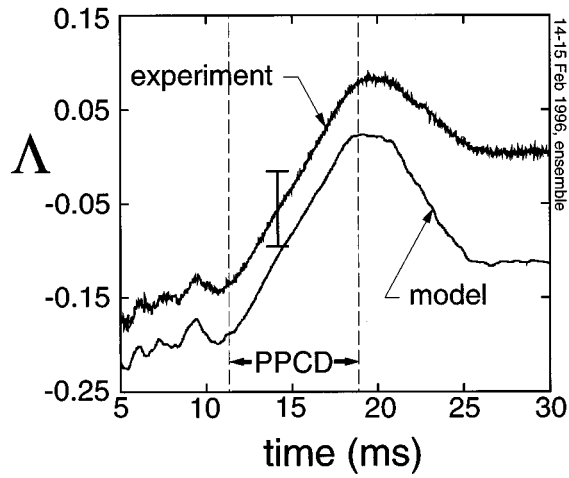Phys. Plasmas, Vol. 4, No. 5, May 1997

Stoneking *et al.* 1635

FIG. 6. The poloidal asymmetry factor measured with an array of 16 field sensing coils for an ensemble of discharges with PPCD applied (top curve), and the prediction for the asymmetry factor from the cylindrical model, using $\Lambda = \beta_\theta - 1 + l_i/2$ (lower curve).
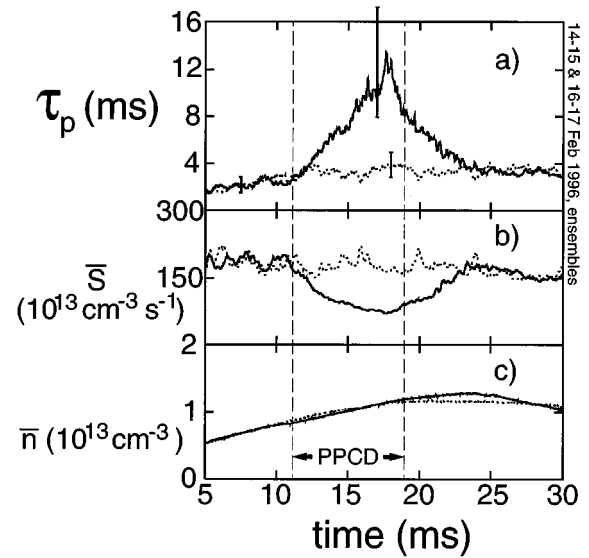

FIG. 7. Ensemble averaged quantities for standard RFP discharges (dashed) and discharges with PPCD applied (solid): (a) particle confinement time, (b) chord averaged ionization source density from H_α radiation, and (c) chord averaged electron density from interferometry.

ing coils at the plasma surface (averaged over 100 discharges with current drive applied), and determined from the relation[18]

$$B_\theta(a,\theta) = B_{\theta 0}\left(1 + \frac{a}{R_0}\,\Lambda\,\cos\,\theta\right). \tag{4}$$

Physically, Λ is determined by the internal inductance and poloidal beta: $\Lambda = \beta_\theta - 1 + l_i/2$ (see, for example, Ref. 18). The experimental observation that the asymmetry factor increases is direct evidence that (1) the normalized plasma pressure increases and/or (2) the internal inductance ($l_i = 2\int B_\theta^2 r dr/a^2 B_{\theta a2}$) increases. In either case, the calculated confinement time is higher for PPCD discharges than without PPCD. As discussed above, the plasma beta increases during PPCD, but the measured increase in beta is not large enough to account for the increase in Λ.

The total inductance [L in Eq. (1)] in the RFP is dominated ($\sim$70%) by the poloidal field contribution that makes up the internal inductance. The measurement of increasing internal inductance (with constant I_ϕ) is evidence that Ohmic power drops during the current drive phase independent of the model used. Because the time derivative of Λ is well reproduced by the model (Fig. 6, lower curve), we are confident that the model quantitatively tracks changes in the total energy inductance, and hence, tracks changes in the stored magnetic energy.

D. Particle confinement

An improvement in the particle confinement time comparable to the observed improvement in energy confinement is inferred from interferometric measurements of plasma density and absolutely calibrated H_α emission measurements. A single collimated H_α detector measures the ionization rate integrated along the line of sight. The detector looks through a central chord into a view dump. The measurement is, therefore, not sensitive to localized sources such as enhanced recycling regions on the wall or puff valves. The calculated particle confinement assumes that the primary par-

ticle source is due to uniform recycling in the edge region. From global particle balance, a particle confinement time is determined from

$$\tau_p = \frac{\bar{n}}{f\bar{S} - d\bar{n}/dt}, \tag{5}$$

where, $\bar{n}$ is the chord averaged plasma density and $\bar{S}$ is the chord averaged ionization rate (per unit volume). The ionization rate is multiplied by a factor, f, that depends on both the plasma density profile and the ionization source profile, and has a value between 1.5 and 2.5 for realistic profiles. The density profile is measured in MST with 11 interferometer chords, but the source profile is not, in general, measured. Figure 7 shows the improvement in particle confinement during PPCD for a profile factor, $f = 2.0 \pm 0.5$. Particle confinement improves by a factor of 4, similar to the observed energy confinement improvement.

The reciprocal of Eq. (5) can be interpreted as a global diffusion coefficient. Locally, it is expected that the radial magnetic fluctuation amplitude governs the diffusion.[19,20] Figure 2 shows a remarkable correlation between the globally inferred diffusion coefficient and the total mean-squared magnetic fluctuation measured at the plasma surface. The absolute scale for diffusion in Fig. 2 requires more detailed profile information. To get order of magnitude values, the relation $D = a^2/4\tau_p$ was used.

IV. CURRENT PROFILE EFFECTS

In the absence of a current profile diagnostic such as the motional Stark effect (MSE), we employ the cylindrical model [Eq. (3)] and measurement of the poloidal asymmetry factor (Fig. 6) to assess effects on the parallel current profile. The model parametrizes the parallel current (normalized to B) through an amplitude, λ_0, and a profile ''flatness'' parameter, α. Large values of α correspond to flat normalized
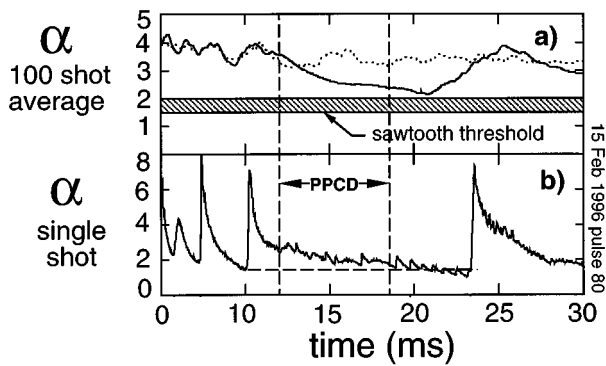
FIG. 8. Profile flatness parameter determined from model [Eq. (3)]. Large values of α indicate a flatter normalized parallel current profile. (a) Profile parameter calculated for an ensemble of standard RFP discharges (dashed) and discharges with PPCD applied (solid). (b) Profile parameter for a single discharge where PPCD was applied at ~12 ms.

parallel current profiles. During the typical sawtooth cycle, the profile varies from an extremely flat $\alpha \sim 8$ immediately after the crash to a peaked $\alpha \sim 2$, which corresponds to a rough threshold for the sawtooth crash. These features can be seen prior to the application of the current drive pulse in Fig. 8 for a single discharge.

To obtain fluctuation suppression and confinement improvement, we find it is not necessary to significantly flatten the current profile, in the sense of increasing α. As shown for the single discharge (Fig. 8), α is not increased; rather the natural rate of profile peaking associated with the sawtooth cycle is slowed. PPCD maintains a current profile that is flatter than the threshold for a sawtooth crash and, thereby, maintains a fluctuation level lower than the sawtooth cycle averaged fluctuation level. After the last of the pulses from the current drive circuit, the profile peaks up leading to a large sawtooth event that terminates the good confinement period. This picture of the effect of PPCD on the current profile comes through in the ensemble of discharges [panel (b)]. The plasma tolerates a more peaked current profile at a lower fluctuation level with PPCD (solid curve) than without PPCD because the applied parallel electric field is better matched to the current profile (times resistivity). Without auxiliary poloidal current drive, the RFP dynamo maintains the configuration through a fluctuation induced parallel electric field (at the $q = 0$ surface, for example, $\langle \tilde{v} \times \tilde{B} \rangle_\parallel = \eta J_\parallel$ without PPCD). The auxiliary applied electric field replaces some of the drive for the parallel current, thereby reducing the fluctuations.

V. CONCLUSIONS

Application of an inductive poloidal electric field to the RFP plasma in MST reduces the fluctuation amplitude asso-

ciated with core resonant tearing modes up to 50%. A coincident improvement in the energy confinement time from 1 to 4 ms occurs in nearly all such discharges. For a subset of discharges where current drive is applied, the fluctuation level reaches record low values (for MST), the confinement time reaches ~5 ms, beta increases from 6% to 9%, and the Ohmic heating power falls by a factor of 3 (Table I). In similar discharges at higher plasma current, we recorded the highest electron temperature measured in MST of 615 eV.

Modeling of the current profile peakedness during these experiments indicates that substantial flattening is not required to produce the observed confinement improvement. This result is encouraging for more steady-state current profile control strategies in the RFP (e.g., electrostatic current injection and rf current drive).

[1] M. R. Stoneking, S. A. Hokin, S. C. Prager, G. Fiksel, H. Ji, and D. J. Den Hartog, Phys. Rev. Lett. **73**, 549 (1994).
[2] G. Fiksel, S. C. Prager, W. Shen, and M. Stoneking, Phys. Rev. Lett. **72**, 1028 (1994).
[3] I. H. Hutchinson, M. Malacarne, P. Noonan, and D. Brotherton-Ratcliffe, Nucl. Fusion **24**, 59 (1984).
[4] R. J. La Haye, T. N. Carlstrom, R. R. Goforth, G. L. Jackson, M. J. Schaffer, T. Tamano, and P. L. Taylor, Phys. Fluids **27**, 2576 (1984).
[5] H. P. Furth, J. Killeen, and M. N. Rosenbluth, Phys. Fluids **6**, 459 (1963).
[6] B. Coppi, J. M. Greene, and J. L. Johnson, Nucl. Fusion **6**, 101 (1966).
[7] D. C. Robinson, Nucl. Fusion **18**, 939 (1978).
[8] Y. L. Ho, Nucl. Fusion **31**, 341 (1991).
[9] E. Uchimoto, M. Cekic, R. W. Harvey, C. Litwin, S. C. Prager, J. S. Sarff, and C. R. Sovinec, Phys. Plasmas **1**, 3517 (1994).
[10] S. Shiina, Y. Kondoh, and H. Ishii, Nucl. Fusion **34**, 1473 (1994).
[11] K. Hattori, Y. Hirano, Y. Yagi, T. Shimada, and K. Hayase, Fusion Technol. **28**, 1619 (1995).
[12] H. Ji, A. F. Almagri, S. C. Prager, and J. S. Sarff, Phys. Rev. Lett. **73**, 668 (1994).
[13] R. N. Dexter, D. W. Kerst, T. H. Lovell, S. C. Prager, and J. C. Sprott, Fusion Technol. **19**, 131 (1991).
[14] S. Hokin, A. Almagri, J. Beckstead, G. Chartas, N. Crocker, M. Cudzinovic, D. J. Den Hartog, R. Dexter, D. Holly, S. Prager, T. Rempel, J. Sarff, E. Scime, W. Shen, C. Spragins, C. Sprott, G. Starr, M. Stoneking, C. Watts, and R. Nebel, Phys. Fluids B **3**, 2241 (1991).
[15] S. Hokin, A. Almagri, M. Cekic, B. Chapman, N. Crocker, D. J. Den Hartog, G. Fiksel, J. Henry, H. Ji, S. Prager, J. Sarff, E. Scime, W. Shen, M. Stoneking, and C. Watts, J. Fusion Energy **12**, 281 (1993).
[16] J. S. Sarff, S. A. Hokin, H. Ji, S. C. Prager, and C. R. Sovinec, Phys. Rev. Lett. **72**, 3670 (1994).
[17] H. Ji, S. C. Prager, A. F. Almagri, J. S. Sarff, Y. Yagi, Y. Hirano, K. Hattori, and H. Toyama, Phys. Plasmas **3**, 1935 (1996).
[18] J. P. Freidberg, *Ideal Magnetohydrodynamics* (Plenum, New York, 1987), p. 122.
[19] J. D. Callen, Phys. Rev. Lett. **39**, 1540 (1977).
[20] A. B. Rechester and M. N. Rosenbluth, Phys. Rev. Lett. **40**, 38 (1978).

Phys. Plasmas, Vol. 4, No. 5, May 1997

Stoneking *et al.*   1637